The Astrophysical Journal Supplement Series, 271:8 (10pp), 2024 March https://doi.org/10.3847/1538-4365/ad159e

Powerful Radio Sources in the Southern Sky. III. First Results of the Optical Spectroscopic Campaign

A. García-Pérez[1,2,3], H. A. Peña-Herazo[4], A. Jimenez-Gallardo[5], V. Chavushyan[1,3], F. Massaro[2,6,7,8], S. V. White[9], A. Capetti[6], B. Balmaverde[6], W. R. Forman[3], C. C. Cheung[10], J. P. Madrid[11], C. Mazzucchelli[12], N. P. H. Nesvadba[13], I. Andruchow[14,15], S. Cellone[15,16], R. Grossová[17,18], A. Paggi[2,6,7], E. Sani[5], V. Reynaldi[15,19], R. P. Kraft[3], and C. Leto[20]

[1] Instituto Nacional de Astrofísica, Óptica y Electrónica, Luis Enrique Erro 1, Tonantzintla, Puebla 72840, Mexico; abigail.garciapz@gmail.com
[2] Dipartimento di Fisica, Università degli Studi di Torino, via Pietro Giuria 1, I-10125 Torino, Italy
[3] Center for Astrophysics | Harvard & Smithsonian, 60 Garden Street, Cambridge, MA 02138, USA
[4] East Asian Observatory (EAO), 660 North A'ohōkū Place, Hilo, HI 96720, USA
[5] European Southern Observatory, Alonso de Córdova 3107, Vitacura, Región Metropolitana, Chile
[6] Istituto Nazionale di Astrofisica (INAF) - Osservatorio Astrofisico di Torino, via Osservatorio 20, I-10025 Pino Torinese, Italy
[7] Istituto Nazionale di Fisica Nucleare (INFN) - Sezione di Torino, via Pietro Giuria 1, I-10125 Torino, Italy
[8] Consorzio Interuniversitario per la Fisica Spaziale, via Pietro Giuria 1, I-10125 Torino, Italy
[9] Department of Physics and Electronics, Rhodes University, PO Box 94, Grahamstown, 6140, South Africa
[10] Space Science Division, Naval Research Laboratory, Washington, DC 20375, USA
[11] Department of Physics and Astronomy, The University of Texas Rio Grande Valley, Brownsville, TX 78520, USA
[12] Instituto de Estudios Astrofísicos, Facultad de Ingeniería y Ciencias, Universidad Diego Portales, Avenida Ejercito Libertador 441, Santiago, Chile
[13] Université de la Côte d'Azur, Observatoire de la Côte d'Azur, CNRS, Laboratoire Lagrange, Boulevard de l'Observatoire, CS 34229, 06304 Nice CEDEX 4, France
[14] Instituto Argentino de Radioastronomía, CONICET-CICPBA-UNLP, CC5 (1897) Villa Elisa, Provincia de Buenos Aires, Argentina
[15] Facultad de Ciencias Astronómicas y Geofísicas, Universidad Nacional de La Plata, Paseo del Bosque, B1900FWA La Plata, Argentina
[16] Complejo Astronómico El Leoncito (CASLEO), CONICET-UNLP-UNC-UNSJ, Avenida España 1512 (sur), J5402DSP San Juan, Argentina
[17] Department of Theoretical Physics and Astrophysics, Faculty of Science, Masaryk University, Kotlářská 2, Brno, CZ-611 37, Czech Republic
[18] Astronomical Institute of the Czech Academy of Sciences, Bocní II 1401, 141 00, Prague, Czech Republic
[19] Instituto de Astrofísica de La Plata (CCT La Plata-CONICET-UNLP), La Plata, Argentina
[20] ASI—Agenzia Spaziale Italiana, Via del Politecnico snc, I-00133 Roma, Italy
Received 2023 July 10; revised 2023 November 13; accepted 2023 November 27; published 2024 February 14

Abstract

We recently built the G4Jy-3CRE catalog of extragalactic radio sources. This catalog lists 264 powerful radio sources selected with similar criteria to those of the revised Third Cambridge Catalog, but visible from the Southern Hemisphere. A literature search revealed that 119 sources in the G4Jy-3CRE catalog (i.e., 45%) lack a firm spectroscopic redshift measurement. Here, we present a campaign aimed at acquiring optical spectra of G4Jy-3CRE sources and measuring their redshifts. We used single-slit observations obtained with the Víctor Blanco Telescope, the New Technology Telescope, the Southern Astrophysical Research Telescope, and the 2.1 m telescope of the Observatorio Astronómico Nacional at San Pedro Mártir, Mexico. In addition, we analyzed Very Large Telescope/MUSE archival observations. From these observations, we report the spectra and redshifts of 93 sources, 42 of which are the first optical spectra and redshift determinations for the respective sources. With our new data, approximately 71% of the sources in the G4Jy-3CRE catalog now have firm spectroscopic redshift measurements. This data set will be the basis of our future analysis of the optical properties of the G4Jy-3CRE catalog.

Unified Astronomy Thesaurus concepts: Extragalactic radio sources (508)

Supporting material: figure set, machine-readable table

1. Introduction

The Third Cambridge Catalogue (3C; Edge et al. 1959) and its revised versions (3CR and 3CRR; Bennett 1962; Laing et al. 1983) list the most powerful radio sources in the sky. The 3C catalog comprises 471 radio sources observed at 159 MHz using the Cambridge Interferometer, while its revised release 3CR (Spinrad et al. 1985) contains 298 extragalactic radio sources. The 3CR sources were selected at $\delta > -5°$ with a nominal flux density >9 Jy at 178 MHz ($\lambda = 1.7$ m).

The 3C, 3CR, and 3CRR catalogs have been a paramount tool for investigating feedback processes occurring in powerful radio sources (Ineson et al. 2013; Kotyla et al. 2016; Ghaffari et al. 2021) and for multiwavelength analyses of extended structures surrounding powerful radio sources (such as jets, hotspots, cavities, shock fronts, knots, and lobes, e.g., Croston et al. 2005; Drouart et al. 2012; Ineson et al. 2013; Mingo et al. 2014; Massaro et al. 2015b; Vagshette et al. 2019; Gill et al. 2021; Jimenez-Gallardo et al. 2021, 2022). The results of most of these analyses have been achieved thanks to the vast suite of observations collected in more than 60 yr of multifrequency campaigns of 3CR sources (see, e.g., Clarke 1964; Law-Green et al. 1995; Hardcastle & Worrall 2000; Massaro et al. 2009, 2010, 2018). However, the 3CR catalog lists mainly sources from the Northern Hemisphere, most of them not

observable by state-of-the-art facilities located in the Southern Hemisphere such as the Atacama Large Millimeter/submillimeter Array (Wootten & Thompson 2009), the MeerKAT radio telescope (see, e.g., Sejake et al. 2023), and the Very Large Telescope (VLT), where observations with modern instruments such as the Multi-unit Spectroscopic Explorer (MUSE) and the Enhanced Resolution Imager and Spectrograph could be obtained. Moreover, upcoming facilities such as the Square Kilometre Array (McMullin et al. 2020), the Large Synoptic Survey Telescope (Ivezić et al. 2019), the Cherenkov Telescope Array, and the Extremely Large Telescope (Gilmozzi & Spyromilio 2007) are also located in the Southern Hemisphere.

Recently, we presented a sample of powerful radio sources extending the 3CR catalog to the Southern Hemisphere: the G4Jy-3CRE catalog (Massaro et al. 2023a, hereinafter Paper I). The G4Jy-3CRE catalog includes 264 sources selected from the Galactic and Extragalactic All-sky Murchison Widefield Array survey (Wayth et al. 2015; Hurley-Walker et al. 2017) having flux densities above 4 Jy at 151 MHz, i.e., the G4Jy catalog (White et al. 2020a, 2020b). Sources listed in the G4Jy-3CRE catalog are those at $\delta < -5^{\circ}$ detected above 9 Jy at ∼178 MHz; thus, this catalog has similar selection criteria as the 3CR at the nominal flux density threshold but lists sources mainly visible from the Southern Hemisphere.

In Paper I we carried out a systematic search for optical counterparts of sources listed in the G4Jy-3CRE catalog comparing archival radio images with better angular resolution than those used for the G4Jy catalog (typically between ∼2′ and 45″; White et al. 2020a, 2020b) with archival optical and infrared images. The radio maps used in Paper I, and the ones in the finding charts presented here, were obtained from the databases of the Very Large Array (VLA) Low-frequency Sky Survey Redux (Cohen et al. 2007), the Tata Institute of Fundamental Research Giant Metrewave Radio Telescope Sky Survey (Intema et al. 2017), the National Radio Astronomy Observatory (NRAO) VLA Sky Survey (Condon et al. 1998), the Sydney University Molonglo Sky Survey (Mauch et al. 2003), the VLA Sky Survey (Lacy et al. 2020), and the NRAO VLA Archive Survey, the latter having angular resolutions between 0.″5 and 10″.[21] Additionally, in Paper I we compared our identified optical counterparts with the mid-infrared (mid-IR) counterparts originally associated in White et al. (2020a, 2020b). Because of our recent work, the fraction of unassociated sources in the G4Jy-3CRE catalog (i.e., sources lacking either an optical or a mid-IR counterpart) is only ∼13%. We also performed a literature search, which allowed us to find reliable spectroscopic redshifts for 145 G4Jy-3CRE sources. Hence, 119 sources lack a reliable spectroscopic redshift measurement, with 66 of them having an optical counterpart listed in Paper I. In the case of the 3CR sample a recent multifrequency analysis of seven unassociated sources, out of the 25 listed in the original catalog (Spinrad et al. 1985), driven by Chandra follow-up observations, allowed us to recognize all their mid-IR counterparts, associated with an optical source in three of the seven cases (Missaglia et al. 2021). A photometric analysis pointed out that three of them could be potential sources at redshifts above ∼1. X-ray emission arising from the northern radio jet of 3C 158 as well as that associated with the radio bridge of 3C 390 was also detected together with that of the intracluster medium around 3C 409 and 3C 454.2.

In Massaro et al. (2023b) (hereinafter Paper II) we presented X-ray archival data from the X-Ray Telescope on board the Neil Gherels Swift satellite for 89 G4Jy-3CRE sources. All these sources had at least one observation with exposure time longer than 250 s. The analysis of these X-ray observations allowed us to investigate the presence of diffuse/extended X-ray emission around G4Jy-3CRE sources, detect X-ray emission from radio lobes, and verify and/or refine the host galaxy identification. After reducing a total of 615 Swift observations, we discovered 61 X-ray counterparts. For 50 of them, we detected an X-ray pointlike counterpart of the radio core while the remaining 11 showed extended X-ray emission. The X-ray results in turn allowed us to confirm the mid-IR counterparts of G4Jy 672 and G4Jy 1192 associated in Paper I and the mid-IR counterpart of G4Jy 1136 found in the original G4Jy catalog (despite the lack of an optical counterpart) and also allowed us to locate the optical counterparts of G4Jy 1192, G4Jy 249, and G4Jy 1432.

Based on the counterpart association and the literature search of spectroscopic redshift measurements described in Paper I, and given the significant fraction of sources lacking a firm spectroscopic redshift, we embarked on an optical spectroscopic campaign to obtain redshift measurements for the entire G4Jy-3CRE catalog, as well as to complete the optical spectroscopic coverage, critical for future multifrequency follow-ups. Thus, in this third paper on the G4Jy-3CRE catalog, we report the first results of our ongoing campaign, which is the first step to achieving a complete characterization of the host galaxies of G4Jy-3CRE sources.

The paper is structured as follows. In Section 2, we present the instrument configurations used and the data reduction procedures adopted. In Section 3, we discuss the results of our optical campaign of the G4Jy-3CRE catalog. Then, in Section 4 we present our conclusions and future research prospects. Finally, in the Appendix we show the spectra and finding charts for all observed targets.

As in Paper I, we adopt cgs units for numerical results and we assume a flat cosmology with $H_0 = 69.6$ km s^{-1} Mpc^{-1}, $\Omega_M = 0.286$, and $\Omega_\Lambda = 0.714$ (Bennett et al. 2014). For optical images, we used those available in the archives of the Panoramic Survey Telescope and Rapid Response System (Pan-STARRS; Flewelling et al. 2020) survey, where magnitudes are reported in the AB system (Oke 1974; Oke & Gunn 1983), or those available in the archives of the Dark Energy Survey (DES; Abbott et al. 2018), for which observations are performed in optical filters similar to those of Pan-STARRS and the Sloan Digital Sky Survey (Ahn et al. 2012a). These were also augmented by images available in the red filter of the Digital Sky Survey[22] (DSS), for all sources outside of the Pan-STARRS and DES footprints.

2. Observations and Data Reduction

Table 1 shows the log of our observations. Sources are listed there using their G4Jy name but we also report a common name if present in the NASA/IPAC Extragalactic Database (NED)[23]

[21] We remark that not all radio observations of the Rapid ASKAP Continuum Survey (McConnell et al. 2020; Hale et al. 2021; Duchesne et al. 2023) had been released when Paper I was in preparation; therefore, these data sets were not included/used there. However, we are currently carrying out an additional investigation on all archival radio observations for the whole G4Jy-3CRE sample that will be presented together with observations recently obtained in a forthcoming paper (F. Massaro et al. 2024, in preparation).

[22] https://archive.eso.org/dss/dss

[23] http://ned.ipac.caltech.edu

Table 1
Log and Results of the Spectroscopic Observations

G4Jy	Common Name	R.A. (J2000)	Decl. (J2000)	IDF	z (Literature)	z (This Work)	σ_z (This Work)	Telescope	UT Date (dd/mm/yyyy)	References
9	⋯	00:05:57.86	−56:28:30.9	1.0	0.2912	0.291	0.001	Blanco	02/12/2022	1
12	⋯	00:06:16.56	−83:06:07.3	1.0	⋯	0.2347	0.0006	NTT	19/11/2022	⋯
48	⋯	00:25:49.17	−26:02:12.8	1.0	0.32188	0.3223	0.0002	Blanco	20/12/2020	2, 3
70	⋯	00:38:26.90	−38:59:47.6	1.0	0.59313	0.594	0.001	Blanco	03/12/2022	1, 4
85	⋯	00:46:17.70	−42:07:51.2	1.0	0.116	0.117	0.001	Blanco	04/12/2022	5
86	NGC 253	00:47:33.16	−25:17:19.6	1.0	0.00081	0.00075	0.00001	VLT	07/11/2018	6
90	⋯	00:50:52.04	−44:28:37.9	1.0	⋯	1.3527	0.0036	NTT	18/11/2022	⋯
93	⋯	00:52:14.90	−43:06:29.4	1.0	⋯	0.3914	0.0004	Blanco	22/08/2021	⋯
113	⋯	01:02:41.72	−21:52:56.8	2.2*	0.0564	0.0566	0.0002	VLT	04/07/2017	7
133	⋯	01:16:25.03	−47:22:41.5	3.0	⋯	0.1478	0.0005	NTT	19/11/2022	⋯
171	NGC 612	01:33:57.88	−36:29:33.8	1.0	0.02977	0.0297	0.0003	Blanco	04/12/2022	8
208	⋯	01:57:41.61	−10:43:41.0	1.0	0.61852	0.616	0.001	OAN-SPM	21/11/2022	1, 9, 10
213	⋯	02:00:12.19	−30:53:27.1	1.0	0.6768	0.678	0.001	SOAR	13/09/2021	11, 12
219	⋯	02:03:40.76	−43:49:51.2	1.0	⋯	0.3602	0.0007	NTT	19/11/2022	⋯
238	3C 62	02:15:37.45	−12:59:30.5	1.0	0.147	0.147	0.001	OAN-SPM	19/11/2022	5
241	⋯	02:16:45.12	−47:49:08.8	1.0	0.064271	0.0642	0.0007	Blanco	02/12/2022	13, 14
249	⋯	02:20:08.06	−70:22:29.4	1.0	⋯	1.160	0.002	SOAR	06/09/2021	⋯
260	⋯	02:25:02.81	−23:12:48.1	1.0	0.232241	0.2324	0.0002	Blanco	16/12/2020	1, 10
290	⋯	02:43:44.26	−51:12:38.5	3.0	⋯	0.7910	0.0013	NTT	20/11/2022	⋯
326	⋯	03:07:31.47	−22:25:14.8	1.0	0.268	0.2718	0.0001	Blanco	13/12/2020	15
347	⋯	03:20:57.30	−45:15:09.3	1.0	0.0622	0.0624	0.0003	Blanco	03/12/2022	16
381	⋯	03:46:30.57	−34:22:46.2	1.0	0.0538	0.0536	0.0004	Blanco	02/12/2022	17
392	3C 94	03:52:30.54	−07:11:02.2	1.0	0.96354	0.965	0.001	OAN-SPM	23/11/2022	10, 18, 19
404	⋯	04:00:16.67	−16:10:11.8	1.0	0.584	0.5835	0.0015	NTT	21/11/2022	10
415	⋯	04:07:48.43	−12:11:36.5	1.0	0.5731	0.5725	0.0016	VLT	25/10/2014	20
427	⋯	04:12:48.13	−56:00:46.3	1.0	⋯	0.4087	0.0003	Blanco	16/12/2020	⋯
462	IC 2082	04:29:08.27	−53:49:40.0	1.0	0.03931	0.0397	0.0003	Blanco	03/12/2022	21, 22, 23
464	⋯	04:29:40.11	−36:30:54.0	1.0	⋯	1.565	0.001	Blanco	15/12/2020	⋯
506	⋯	04:55:14.43	−30:06:46.0	1.0	⋯	0.1349	0.0004	Blanco	13/12/2020	⋯
510	⋯	04:56:08.93	−21:59:09.2	1.0	0.533	0.533	0.001	Blanco	12/04/2022	24, 25, 26
517	⋯	05:05:49.24	−28:35:19.4	1.0	0.0381	0.0380	0.0003	Blanco	02/12/2022	1, 27, 28, 29
518	⋯	05:06:44.10	−61:09:41.0	1.0	1.093	1.0861	0.0004	VLT	01/12/2019	26, 30
524	⋯	05:10:31.95	−18:38:44.0	2.1	⋯	0.2087	0.0001	Blanco	17/12/2020	⋯
530	⋯	05:12:47.36	−48:24:16.2	2.2*	0.30638	0.3066	0.0003	Blanco	02/12/2022	31
531	⋯	05:13:31.98	−30:28:49.7	1.0	0.05764	0.0576	0.0005	Blanco	13/04/2022	1
540	⋯	05:22:57.98	−36:27:31.3	1.0	0.056546	0.0556	0.0005	Blanco	03/12/2022	1, 32
563	⋯	05:36:13.62	−49:44:26.2	1.0	⋯	0.1853	0.0004	NTT	18/11/2022	⋯
590	⋯	06:03:12.23	−34:26:32.8	1.0	⋯	0.5384	0.0027	NTT	18/11/2022	⋯
605	⋯	06:20:01.00	−37:11:43.1	1.0	⋯	0.0323	0.0003	NTT	21/11/2022	⋯
607	⋯	06:21:43.37	−52:41:34.1	1.0	0.051	0.0497	0.0005	Blanco	03/12/2022	33
613	⋯	06:26:49.56	−54:32:34.1	1.0	0.051976	0.0524	0.0006	Blanco	03/12/2022	34
614	⋯	06:27:06.78	−35:29:16.8	1.0	0.054855	0.0549	0.0001	Blanco	13/12/2020	1, 5, 35
629	⋯	06:48:11.16	−39:57:11.5	1.0	⋯	0.2343	0.0001	Blanco	15/12/2020	⋯
642	⋯	07:05:54.29	−42:48:53.8	1.0	⋯	1.333	0.002	Blanco	17/12/2020	⋯
644	⋯	07:09:14.10	−36:01:25.0	1.0	0.110	0.1108	0.0002	Blanco	03/12/2022	36
653	⋯	07:20:15.06	−55:25:20.1	1.0	⋯	0.2186	0.0012	NTT	20/11/2022	⋯
680	⋯	08:02:36.26	−09:57:39.8	2.2*	0.0699	0.0714	0.0004	Blanco	13/04/2022	37
721	3C 206	08:39:50.57	−12:14:33.4	1.0	0.19787	0.198	0.001	Blanco	12/04/2022	38
747	⋯	09:01:47.26	−25:55:16.0	1.0	0.305	0.3050	0.0001	Blanco	20/12/2020	5
779	⋯	09:38:01.43	−29:12:36.2	1.0	⋯	0.1984	0.0004	Blanco	14/12/2020	⋯
854	⋯	10:33:13.14	−34:18:45.2	4.3	⋯	0.4873	0.0003	SOAR	02/03/2020	⋯
917	⋯	11:25:52.97	−35:23:40.4	1.0	0.033753	0.0322	0.0005	Blanco	13/04/2022	8, 33, 39, 40
927	⋯	11:34:23.69	−17:27:50.3	1.0	1.618	1.620	0.002	SOAR	10/03/2022	10
934	⋯	11:39:16.90	−32:22:20.9	3.0	⋯	0.633	0.001	NTT	09/06/2021	⋯
950	⋯	11:45:31.07	−48:36:11.2	1.0	⋯	0.3666	0.0019	NTT	19/11/2022	⋯
986	⋯	12:18:06.28	−46:00:29.4	1.0	⋯	0.527	0.001	SOAR	27/03/2022	⋯
987	⋯	12:18:38.10	−10:20:35.0	1.0	0.0874	0.0867	0.0001	Blanco	12/04/2022	10, 37
1035	⋯	12:54:40.99	−29:13:39.5	1.0	0.057353	0.0584	0.0021	NTT	09/06/2021	41, 42
1038	3C 279	12:56:11.15	−05:47:21.9	1.0	0.5362	0.535	0.001	SOAR	07/05/2022	43
1071	⋯	13:30:07.13	−21:42:01.7	1.0	0.528	0.5248	0.0003	Blanco	12/04/2022	10, 44

Table 1
(Continued)

G4Jy	Common Name	R.A. (J2000)	Decl. (J2000)	IDF	z (Literature)	z (This Work)	σ_z (This Work)	Telescope	UT Date (dd/mm/yyyy)	References
1072	⋯	13:31:08.65	−25:59:44.6	1.0	⋯	1.214	0.001	Blanco	12/04/2022	⋯
1079	⋯	13:34:18.66	−10:09:27.6	1.0	⋯	0.0836	0.0005	Blanco	13/04/2022	⋯
1080	IC 4296	13:36:38.94	−33:57:57.7	1.0	0.0125	0.01232	0.00016	VLT	11/04/2016	39
1083	4C-06.35	13:38:07.97	−06:27:11.1	1.0	0.625	0.623	0.001	NTT	11/06/2021	44
1093	⋯	13:47:01.46	−08:03:23.2	1.0	0.384	0.383	0.001	SOAR	26/04/2022	10
1152	⋯	14:22:49.22	−27:27:56.6	1.0	0.985	0.9784	0.0003	VLT	23/02/2020	45
1172	⋯	14:28:57.12	−48:12:09.4	1.0	⋯	0.0738	0.0005	SOAR	07/06/2021	⋯
1187	⋯	14:42:02.27	−26:37:19.3	1.0	⋯	0.2457	0.0001	SOAR	01/07/2021	⋯
1197	⋯	14:52:35.30	−13:11:20.7	2.1	⋯	0.0694	0.0006	Blanco	13/04/2022	⋯
1209	⋯	14:55:54.89	−11:08:43.5	1.0	0.942	0.939	0.001	Blanco	13/04/2022	46
1225	4C-05.64	15:10:53.59	−05:43:07.3	1.0	1.191	1.1850	0.0004	VLT	22/02/2022	47
1279	⋯	15:48:57.97	−32:16:57.9	1.0	0.1082	0.1085	0.0003	NTT	09/06/2022	48
1360	⋯	16:44:16.06	−77:15:49.7	1.0	0.0427	0.0424	0.0004	Blanco	05/04/2021	48
1432	⋯	17:42:01.43	−60:55:12.4	1.0	⋯	0.145	0.001	SOAR	31/05/2021	⋯
1497	⋯	18:36:59.51	−66:49:09.0	1.0	⋯	0.247	0.001	NTT	18/11/2022	⋯
1498	⋯	18:37:41.47	−43:35:41.4	2.2	⋯	0.412	0.001	SOAR	07/05/2022	⋯
1505	⋯	18:44:28.87	−40:22:01.3	4.1	⋯	0.657	0.001	NTT	09/06/2022	⋯
1530	⋯	19:21:52.49	−54:31:57.4	1.0	⋯	0.3091	0.0013	NTT	20/11/2022	⋯
1546	⋯	19:30:01.92	−15:09:19.5	1.0	⋯	0.0815	0.0010	NTT	10/06/2021	⋯
1569	⋯	19:43:51.68	−40:30:13.5	1.0	⋯	0.202	0.001	SOAR	13/07/2021	⋯
1637	⋯	20:33:52.79	−73:03:57.4	1.0	⋯	0.456	0.005	NTT	21/11/2022	⋯
1678	⋯	21:07:25.63	−25:25:43.4	1.0	0.03881	0.0383	0.0005	Blanco	13/04/2022	5, 49
1708	⋯	21:37:45.18	−14:32:55.8	1.0	0.20047	0.20021	0.00019	VLT	03/06/2016	38, 50
1717	⋯	21:43:33.42	−43:12:53.1	1.0	⋯	0.648	0.001	SOAR	13/07/2021	⋯
1756	⋯	22:05:04.87	−55:17:43.8	1.0	⋯	0.661	0.001	SOAR	29/08/2021	⋯
1757	⋯	22:06:10.41	−18:35:38.6	1.0	0.6185	0.620	0.001	NTT	09/06/2021	51, 52
1780	⋯	22:27:02.40	−52:33:24.7	1.0	⋯	0.454	0.001	Blanco	21/08/2021	⋯
1799	⋯	22:56:47.37	−51:58:44.4	3.0	⋯	0.4614	0.0003	NTT	11/06/2022	⋯
1801	⋯	23:02:24.23	−37:18:07.7	4.1	⋯	0.1912	0.0004	NTT	11/06/2022	⋯
1819	⋯	23:19:56.30	−27:28:12.3	1.0	⋯	0.1746	0.0009	NTT	20/11/2022	⋯
1824	⋯	23:22:06.82	−54:45:30.5	1.0	⋯	0.878	0.002	NTT	19/11/2022	⋯
1829	⋯	23:25:19.77	−12:07:27.3	1.0	0.082991	0.0820	0.0002	VLT	11/10/2014	1, 7, 53, 54
1858	⋯	23:57:00.85	−34:45:35.0	1.0	0.04981	0.0494	0.0011	VLT	21/10/2014	1

Notes. Sources marked with * next to their IDF are those for which the mid-IR counterpart was identified in the refined optical analysis of Paper I. References: (1) Jones et al. (2009); (2) Holt et al. (2008); (3) Santoro et al. (2020); (4) Thompson et al. (1990); (5) Tadhunter et al. (1993); (6) Springob et al. (2005); (7) Owen et al. (1995); (8) Burbidge & Burbidge (1972); (9) Burbidge (1968); (10) Best et al. (1999); (11) Croom et al. (2004); (12) Jones et al. (2004); (13) Abell (1958); (14) Abell et al. (1989); (15) McCarthy et al. (1996); (16) Safouris et al. (2009); (17) Scarpa et al. (1996); (18) Lynds (1967); (19) Ahn et al. (2012); (20) Kinman & Burbidge (1967); (21) Jones & McAdam (1992); (22) Burgess & Hunstead (2006); (23) White et al. (2020a); (24) Wright et al. (1979); (25) Henriksen et al. (1991); (26) Bechtold et al. (2002); (27) Menzies et al. (1989); (28) Fouque et al. (1990); (29) da Costa et al. (1991); (30) Wright et al. (1977); (31) Eracleous & Halpern (2004); (32) Sbarufatti et al. (2006); (33) Tritton (1972); (34) Cava et al. (2009); (35) Wills et al. (2004); (36) Parisi et al. (2014); (37) Danziger & Goss (1983); (38) Ho & Kim (2009); (39) Sandage (1978); (40) Allison et al. (2014); (41) Melnick & Quintana (1981); (42) Kaldare et al. (2003); (43) Marziani et al. (1996); (44) Burbidge & Kinman (1966); (45) Goncalves et al. (1998); (46) Schmidt (1966); (47) Peterson & Bolton (1972); (48) Simpson et al. (1993); (49) Garilli et al. (1993); (50) Baldwin (1975); (51) Stickel et al. (1989); (52) Morton & Tritton (1982); (53) Schmidt (1965); (54) Costero & Osterbrock (1977).

(This table is available in machine-readable form.)

and/or in SIMBAD.[24] It is worth noting that radio cross-identifications for all the G4Jy-3CRE sources are listed in Appendix B of Paper I. Table 12 of Paper I reports the G4Jy name together with the name associated in the following radio catalogs: the Parkes radio catalog (PKSCAT90; Bolton et al. 1979), the Molonglo Reference Catalog of Radio Sources (Large et al. 1981), the Parkes-MIT-NRAO catalog (Griffith & Wright 1993; Wright et al. 1994), the Texas survey of discrete radio sources (Douglas et al. 1996), and the Australia Telescope 20 GHz Survey (Murphy et al. 2010), mainly covering the Southern Hemisphere. It also lists those objects associated with Abell galaxy clusters.

The optical spectra presented here were collected at the Víctor Blanco Telescope, the New Technology Telescope (NTT), the Southern Astrophysical Research (SOAR) Telescope, and the 2.1 m Telescope of the Observatorio Astronómico Nacional located at San Pedro Mártir, Mexico (OAN-SPM). Details for each facility are reported below, along with the archival data from VLT. We adopted the same data reduction procedure successfully used in previous optical campaigns (see, e.g., Massaro et al. 2015a; Peña-Herazo et al. 2017, 2019, 2021; García-Pérez et al. 2023), as well as a similar setup for all

[24] http://simbad.u-strasbg.fr/simbad/

instruments used (see, e.g., Landoni et al. 2015; Ricci et al. 2015). Here, we only summarize the main steps of the data reduction. Additional information can be obtained from the papers mentioned above.

2.1. Víctor Blanco

Forty-two sources were observed with the Blanco 4 m telescope located at the Cerro Tololo Inter-American Observatory, Chile (proposal ID 2021B-0901, PI: F. Massaro; proposal ID 2022B-577686, PI: H. Pena). We used the COSMOS spectrograph with the red grism (r2k), a 1.″2 slit width at the blue position, and the GG495 filter. This setup provided a spectral coverage between 5000 and 9075 Å and a dispersion of 1 Å pixel^{-1}. We acquired HgNe comparison lamp spectra on each target position for wavelength calibration.

2.2. NTT

Thirty-five sources were observed at the NTT (proposal ID 110.23Q3.001, PI: A. Jimenez-Gallardo; proposal ID 105.205K.001, PI: F. Ricci). We performed long-slit spectroscopic observations using the EFOSC2 spectrograph with grism No. 13 and a slit width of 1″. This instrument configuration covered the spectral range between 3700 and 9000 Å and a dispersion of 2.77 Å pixel^{-1}. After each target, we observed HeAr comparison lamps to perform wavelength calibration.

2.3. SOAR

Twenty-eight sources were observed with the 4.1 m SOAR Telescope (proposal ID SOAR2020A-002, SOAR2021B-001, and SOAR2022A-013, PI: F. Massaro) located in Cerro Pachón, Chile. We used the single, long-slit mode of the Goodman High Throughput Spectrograph (Clemens et al. 2004) with a slit width of 1″ and a grating of 400 lines mm^{-1}, giving a dispersion of ∼3 Å pixel^{-1} in a spectral range of ∼4100 Å to 7900 Å, and a resolution of ∼6 Å. We obtained HgArNe arcs to perform wavelength calibration.

2.4. OAN-SPM 2.1 m Telescope

Three sources were observed with the 2.1 m telescope of OAN-SPM (proposal ID 25, PI: A. García-Pérez). We made use of the Boller and Chivens spectrograph with a 1024 × 1024 pixel E2V 4240 CCD, tuned to the 4000–8000 Å range, providing a dispersion of 2.26 Å pixel^{-1} with a slit width of 2.″5. This configuration resulted in a spectral resolution of 10 Å. Wavelength calibration was performed using CuHeNeAr comparison lamps.

2.5. VLT

Eleven G4Jy-3CRE sources have publicly available VLT data obtained with MUSE (Bacon et al. 2010) in the ESO archive.[25] These observations were taken in wide-field mode with natural seeing, which samples a ∼1 arcmin^2 field of view with 0.″2 spatial pixels. MUSE provides a spectral range of 4800–9300 Å and a dispersion of 2.51 Å pixel^{-1}.

We obtained fully reduced and calibrated data cubes from the ESO archive. Optical spectra were extracted from a circular region with radii chosen to match the seeing, typically ∼1″, centered on the host position (see Paper I for details on the host association). It is worth noting that, although these are VLT archival observations from between 2014 and 2022, the literature redshifts reported in Table 1 correspond to spectra obtained at other telescopes.

Five of the 11 sources with VLT/MUSE archival data were reobserved during our campaign. For those cases, we chose as the final redshift measurement the one obtained with VLT/MUSE due to its higher signal-to-noise ratio (S/N) and spectral resolution, except for G4Jy 1035. For this source, the spectrum from the NTT has a higher S/N and the broader spectral range allowed us to identify more spectral features.

2.6. Data Reduction

We carried out the data reduction using `IRAF` packages (Tody 1986). First, for each acquisition, we performed bias subtraction and flat-field correction. Different exposures of individual sources were combined using the task median, which allowed us to reject most of the cosmic rays. We performed wavelength calibration using comparison arcs taken for each object. Flux calibration was performed using standard stars observed during the same nights as our science spectra. The final spectra are shown in the Appendix, along with the finding charts of each source. Additionally, in the Appendix we report the mean S/N of each spectrum. The S/N of each spectrum was measured with IRAF, considering wavelength intervals where only continuum emission was present (without any spectral features) and was located at the center of the wavelength range of each spectrum.

We inspected each spectrum to identify the most common spectral lines, ranging from C IV, Mg II, and [O II] to Hα, [N II], and [S II] in emission, and absorption features such as Ca II K and H, the *G* band, Mg I, and Na I. A Gaussian profile was fitted to all emission and absorption lines of each spectrum. We used the center wavelengths to derive the redshift with each line and then we calculated the mean. For the uncertainties (σ_z), we computed the standard deviation of the redshift values obtained with each line. In the cases of G4Jy 464, G4Jy 642, and G4Jy 1717, to obtain the center wavelength of the Mg II emission line, a more robust fit was performed considering the absorption features affecting it. In particular, the spectrum of G4Jy 464 exhibits only this line. Therefore, to calculate σ_z for this source, we performed uncertainty propagation, using the center wavelength and its uncertainty, both derived from the fit.

3. Results

We obtained new spectra for 93 radio sources of the G4Jy-3CRE catalog, most of them with high S/N. With the new optical spectra, we derived the redshifts for these objects. All results of our analysis are summarized in Table 1.

For 42 of the 93 sources analyzed here, for the first time, we report a spectroscopic redshift measurement. For the remaining 51 sources, our redshift measurements are consistent with the literature redshifts retrieved in Paper I, within a 3σ statistical uncertainty, except for nine cases, namely G4Jy 86, G4Jy 518, G4Jy 644, G4Jy 680, G4Jy 917, G4Jy 1071, G4Jy 1152, G4Jy 1225, and G4Jy 1829. For G4Jy 518, G4Jy 644, G4Jy 1071, and G4Jy 1152 the differences are mostly related to the higher precision of our measurements, while for G4Jy 917 and G4Jy 1829 the literature redshifts possess a higher precision. For G4Jy 86, we extracted the spectrum from the circumnuclear

[25] http://archive.eso.org/scienceportal/home

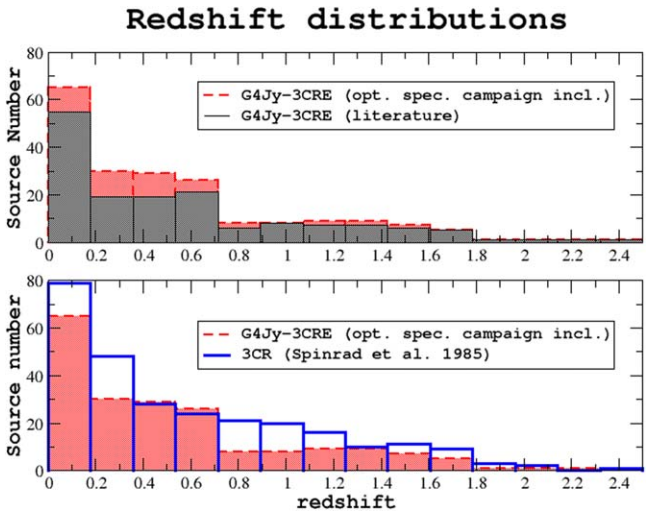

Figure 1. Upper panel: comparison between redshifts obtained during our literature search from Paper I (gray) and including all the redshifts that we now have thanks to our campaign (red). Lower panel: we show the distribution of redshifts for sources of the G4Jy-3CRE catalog (red) in comparison with that of the 3CR catalog (blue).

region of the galaxy since the precise location of the nucleus is unclear. We measured the redshift from the Ca II triplet absorption lines and obtained $z = 0.00075 \pm 0.00001$ consistent with the literature value $z = 0.00081$ (Springob et al. 2005). The redshift measurement for this source is affected by the kinematics of several star-forming clumps surrounding the nucleus. Hence, when measuring the redshift from the emission lines (most likely associated with these regions) we obtain $z = 0.00035 \pm 0.00016$. Sources G4Jy 680 and G4Jy 1225 are discussed in Section 3.2.

Considering both the literature redshifts and the redshifts obtained here, we now have firm redshift measurements for 187 out of the 264 G4Jy-3CRE sources. In Figure 1 (upper panel) we show their redshift distribution, which ranges from 0.00075 to 2.34665, where most of the values are $z \lesssim 0.6$. In addition, in Figure 1 (lower panel) we compare the redshifts of the 187 sources from the G4Jy-3CRE catalog with those of the 3CR catalog, showing that the redshift values from both catalogs are similarly distributed.

3.1. Identification Flags

In Paper I we adopted identification flags (IDFs) to characterize the counterpart associations (see the detailed explanation of each IDF in Paper I). The G4Jy-3CRE sources having an optical and mid-IR counterpart associated were labeled as IDF = 1, while those having an optical counterpart that was different from the mid-IR counterpart or lacking the latter were labeled as IDF = 2.1 or 2.2, respectively. The associations with mid-IR counterparts, detected in the all-sky survey performed with the Wide-field Infrared Survey Explorer (WISE; Wright et al. 2010), were carried out for the entire G4Jy catalog in White et al. (2020a, 2020b). In Paper I we adopted IDF = 2.2 for those sources having the identification of the host galaxy partially or completely limited by the mid-IR data, with the galaxy either undetected in the AllWISE survey or having its emission affected by a relatively bright nearby object. However, the refined analysis of optical counterparts carried out in Paper I allowed us to discover the WISE counterpart for 12 additional sources previously listed with IDF = 2.2, three of them also present here in our optical campaign, namely G4Jy 113, G4Jy 530, and G4Jy 680. Sources for which we could not uniquely identify one optical counterpart were labeled as IDF = 3. Finally, we labeled as IDF = 4 sources that we were not able to associate with an optical counterpart but possessed a mid-IR counterpart already associated in the original G4Jy catalog (IDF = 4.1), sources that we were not able to associate with an optical counterpart but were associated with an incorrect mid-IR counterpart according to our radio maps (IDF = 4.2), and sources that lacked both counterparts (IDF = 4.3).

Of the 93 sources for which we obtained redshifts, 80 have an IDF equal to 1, corresponding to sources with optical and mid-IR counterparts coincident with the radio core. Here, for the first time, we provide spectroscopic redshifts for 32 counterparts with IDF = 1.

We observed the optical counterparts reported in Paper I of two sources with IDF = 2.1 (G4Jy 524 and G4Jy 1197) and four with IDF = 2.2 (G4Jy 113, G4Jy 530, G4Jy 680, and G4Jy 1498). For three of these IDF = 2.1 and IDF = 2.2 sources, we provide the first redshift measurements.

Four of the observed sources have IDF = 3.0, namely G4Jy 133, G4Jy 290, G4Jy 934, and G4Jy 1799. For these cases, where no clear optical counterpart was associated in Paper I, we observed the sources marked in their finding charts (Appendix). The coordinates are reported in Table 1.

We observed two sources with IDF = 4.1 (G4Jy 1505 and G4Jy 1801), and one with IDF = 4.3 (G4Jy 854). For these cases, we also report the observed sources and their coordinates, since these cases have no optical counterpart previously associated.

In order to associate the optical counterparts for the aforementioned sources from cases IDF = 3 and IDF = 4, we considered the procedure employed in Paper I. These sources show a spectrum like that of an active galactic nucleus (AGN), and the probability of finding several radio-loud AGN per square degree of the sky is low, which further supports our association.

3.2. Literature Search

For the radio source G4Jy 1225, observed with the NTT and with VLT/MUSE archival data, we obtained a redshift measurement of $z = 1.1857 \pm 0.0002$ with the NTT and $z = 1.1850 \pm 0.0004$ with VLT/MUSE. This redshift was marked as uncertain in Paper I since we incorrectly reported the redshift measurement from Torrealba et al. (2012), which is in fact $z = 1.191$. Moreover, after a new literature check, we found both the spectrum and line measurements reported for this source, with $z = 1.186$ (Wilkes et al. 1983; Wilkes 1986). The redshifts reported in the literature are consistent with our measurement. It is worth noting that in comparison to the spectra available in the literature, we identified more emission lines in our spectrum since it covers a different spectral range, thus enabling us to obtain a more refined redshift.

For G4Jy 85 we obtained $z = 0.117 \pm 0.001$, which is in agreement with the value $z = 0.116$ found during our literature search (Tadhunter et al. 1993). In Paper I, we reported this redshift as 0.0526 from Whiteoak (1972), but the actual spectrum was not published. On the other hand, Tadhunter et al. (1993) reported both the spectrum and a description of it.

In all future papers of the series, the flag reported for G4Jy 1225 with the literature redshift $z = 1.191$, as well as the

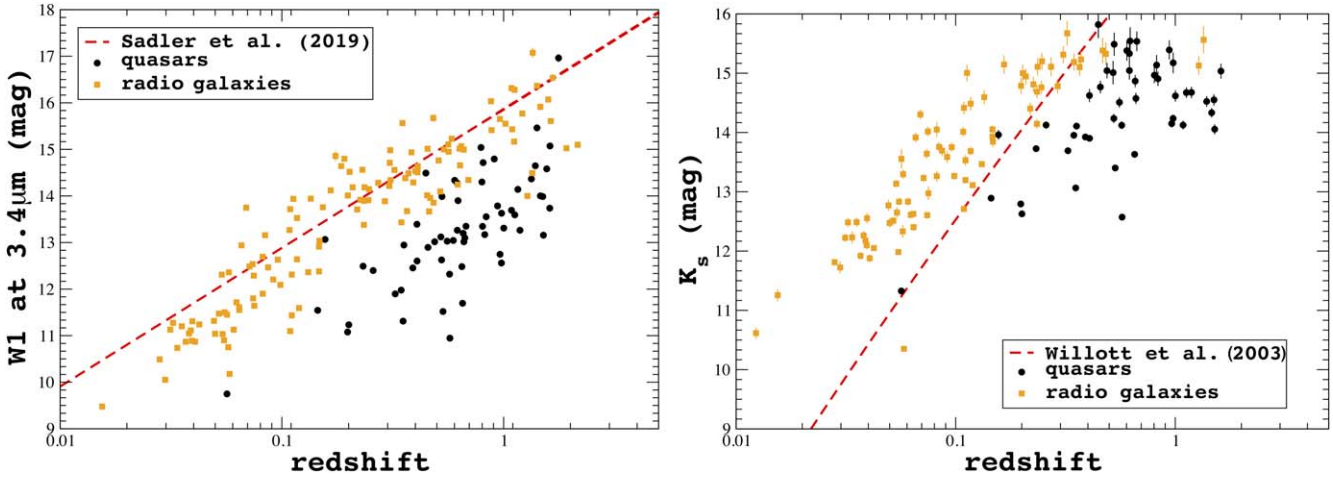

Figure 2. Left panel: relation between 3.4 μm AllWISE magnitudes and the redshifts of 189 sources of the G4Jy-3CRE catalog. Right panel: same as left panel, but using K_s magnitudes from 2MASS instead, for 128 sources.

literature measurement for G4Jy 85 correspondent to $z = 0.116$, will be appropriately corrected. This also applies to Paper II.

In the case of G4Jy 680, the optical spectrum is not available in the literature; only the identified lines are reported (Danziger & Goss 1983). We consider our redshift measurement to be more reliable since we were able to identify more spectral features in our spectrum to derive the redshift.

3.3. *Infrared Magnitude versus* z *Relation*

Sources listed in the 3CRR exhibit a tight relation between their *K*-band magnitudes and redshifts (Laing et al. 1983; Lilly & Longair 1984). This relation has been found up to $z = 3$ in other complete samples and suggests that the stellar populations of radio galaxy hosts formed at high redshifts and have evolved passively up to the present (see, e.g., Jarvis et al. 2001; Willott et al. 2003; Rocca-Volmerange et al. 2004). We plotted K_s magnitudes versus z in order to verify whether G4Jy-3CRE sources follow this trend and thus assess the reliability of our counterpart associations. We distinguished the radio sources of the G4Jy-3CRE between quasars and radio galaxies using both the optical spectra reported in the present paper and those that were retrieved in the literature and for which all notes are available in Paper I.

In the left panel of Figure 2 we show the magnitude–z relation for a total of 189 radio sources (i.e., 61 quasars and 128 radio galaxies) computed using the infrared magnitude measured in the W1 band of the AllWISE sky survey (Wright et al. 2010) at 3.4 μm while in the right panel we report the relation using the K_s magnitude available from the Two Micron All Sky Survey (2MASS) for 48 quasars and 80 radio galaxies. In both left and right panels, we also report the relations drawn from Sadler et al. (2019) and Willott et al. (2003), respectively. Despite the fact that these relations were mainly derived for relatively high z radio samples, in the magnitude$-z$ diagrams radio galaxies tend to be more in agreement with these trends while quasars, having their infrared magnitude contaminated by nonthermal emission, tend to be brighter than expected.

4. Summary and Conclusions

Here we present the results of our observing campaign carried out between 2020 March and 2022 December to obtain optical spectra and redshift measurements for sources in the G4Jy-3CRE catalog. From these observations, we derived redshifts for 93 sources. For 42 of them, we publish the first optical spectra, while for the remaining 51 we were able to confirm previous redshifts available in the literature. Archival optical spectra for these 51 sources were not available in the literature. Thus, the newly obtained optical spectra will allow us to carry out their classification.

Currently, thanks to this campaign and to the literature search carried out in Paper I, 187 sources out of the 264 listed in the G4Jy-3CRE catalog have firm spectroscopic redshift measurements (which represent roughly 71% of the whole catalog) while the redshifts for 11 sources remain uncertain, as marked in Paper I.

Additionally, in Paper I we built a subsample of sources having flux densities above 9.8 Jy at 178 MHz, comprising 181 radio sources. This subsample was created to account for intercalibration issues between radio flux density measurements of the 3C and subsequent observations, and is therefore a closer equivalent to the 3CR (see Paper I and references therein). Considering exclusively our subsample, we currently have firm spectroscopic redshift measurements for 137 out of 181 radio sources, and five sources with uncertain redshifts according to our literature search, thus achieving a redshift coverage of 75% of the G4Jy-3CRE subsample.

In our forthcoming paper of the G4Jy-3CRE series, we will present the optical spectra and redshift measurements for the remaining sources of the sample, as well as those for targets with redshift measurements marked as uncertain in Paper I (e.g., new spectra will become available via follow-up on the Southern African Large Telescope; proposal ID 2020-1-210-MLT-008, PI: White). Finally, we will use all optical spectra collected to classify all the sources in the G4Jy-3CRE catalog, crucial to analyzing differences among radio source populations. The optical continuum will be subtracted from the spectra. Then, we will measure equivalent widths and line fluxes, allowing us to obtain line ratios and create diagnostic diagrams to distinguish between low-excitation radio galaxies, high-excitation radio galaxies, quasars, and star-forming galaxies (see, e.g., Hine & Longair 1979; Laing et al. 1994; Buttiglione et al. 2010; Baldi et al. 2019).

Acknowledgments

We wish to dedicate this paper to D. E. Harris and R. W. Hunstead—their insight, passion, and contribution to radio astronomy are an inspiration to us. A.G.-P. acknowledges support from the CONAHCyT program for her PhD studies and support from the Center for Astrophysics | Harvard & Smithsonian during her enrollment in the fellows program. V. C. acknowledges support from the Fulbright-García Robles scholarship. This work was partially supported by CONACyT (Consejo Nacional de Ciencia y Tecnología) research grant 280789 (Mexico). S.V.W. acknowledges financial assistance of the South African Radio Astronomy Observatory (SARAO).[26] W.R.F. and R.P.K. acknowledge support from the Smithsonian Institution and the Chandra High Resolution Camera Project through NASA contract NAS8-03060. W.R.F. also acknowledges support from NASA grants 80NSSC19K0116, GO1-22132X, and GO9-20109X. This investigation is supported by the National Aeronautics and Space Administration (NASA) grants GO9-20083X, GO0-21110X, and GO1-22087X. I.A., S.C., and V.R. are partially supported by grant PIP 1220200102169CO, Argentine Research Council (CONICET), and by the UNLP research project G178 (2022–2025). C.C.C. was supported at the Naval Research Laboratory by NASA DPR S-15633-Y. Supported by the Italian Research Center on High Performance Computing Big Data and Quantum Computing (ICSC), project funded by European Union—NextGenerationEU—and National Recovery and Resilience Plan (NRRP) Mission 4 Component 2 within the activities of Spoke 3 (Astrophysics and Cosmos Observations). Based on observations obtained at the SOAR Telescope, which is a joint project of the Ministério da Ciência, Tecnologia, e Inovação (MCTI) da República Federativa do Brasil, the US National Optical Astronomy Observatory (NOAO), the University of North Carolina at Chapel Hill, and Michigan State University. Based on observations collected at the European Southern Observatory under ESO program 110.23Q3.001 and data obtained from the ESO Science Archive Facility with DOIs under https://doi.org/10.18727/archive/41 and https://doi.org/10.18727/archive/42. Based on observations made at Cerro Tololo Inter-American Observatory at NSF's NOIRLab (proposal ID 2021B-0901, PI: F. Massaro; proposal ID 2022B-577686, PI: H. Pena), which is managed by the Association of Universities for Research in Astronomy (AURA) under a cooperative agreement with the National Science Foundation. Based on observations carried out at the Observatorio Astronómico Nacional on Sierra San Pedro Mártir (OAN-SPM), Baja California, Mexico.

This research has made use of NED, which is operated by the Jet Propulsion Laboratory, California Institute of Technology, under contract with the National Aeronautics and Space Administration. This research has made use of the SIMBAD database, operated at CDS, Strasbourg, France (Wenger et al. 2000). This research has made use of the cutout service at cutouts.cirada.ca, operated by the Canadian Initiative for Radio Astronomy Data Analysis (CIRADA). CIRADA is funded by a grant from the Canada Foundation for Innovation 2017 Innovation Fund (Project 35999), as well as by the Provinces of Ontario, British Columbia, Alberta, Manitoba, and Quebec, in collaboration with the National Research Council of Canada, the US National Radio Astronomy Observatory, and Australia's Commonwealth Scientific and Industrial Research Organisation. SAOImageDS9 development has been made possible by funding from the Chandra X-Ray Science Center, the High Energy Astrophysics Science Archive Research Center (HEASARC), and the JWST Mission Office at the Space Telescope Science Institute (Joye & Mandel 2003). This research has made use of data obtained from HEASARC provided by NASA's Goddard Space Flight Center. We acknowledge the use of NASA's SkyView facility[27] located at NASA's Goddard Space Flight Center. The TOPCAT and STILTS astronomical software (Taylor 2005) were used for the preparation and manipulation of the tabular data and the images. The analysis is partially based on the OCCAM computing facility hosted by C3S[28] at UniTO (Aldinucci et al. 2017).

Appendix
Optical Spectra and Finding Charts

In this appendix, we show the optical spectra and the finding charts of the 93 sources analyzed in this work (Figure 3).

[26] https://www.sarao.ac.za

[27] http://skyview.gsfc.nasa.gov

[28] http://c3s.unito.it/

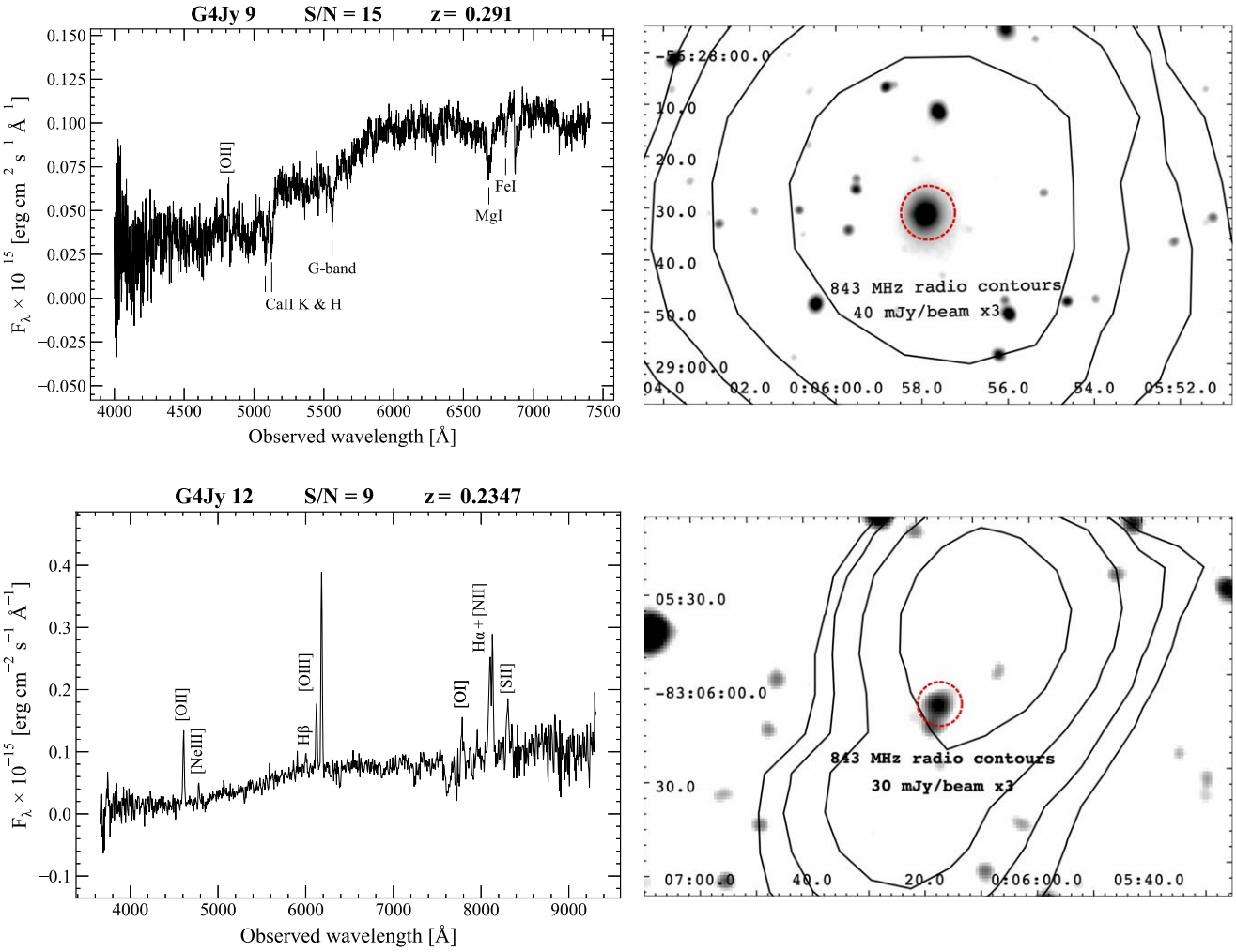

Figure 3. Left panel: optical spectrum of each G4Jy-3CRE source obtained in this campaign. Identified emission and absorption lines are labeled. On top of each spectrum, we show the name of the source, the mean S/N of the spectrum, and the redshift obtained. Right panel: the corresponding finding chart for each source, retrieved from the DSS archive, Pan-STARRS database, or DES database. Radio contours are overlaid in black (for more details see Paper I). The symbol x3 reported in each finding chart indicates that the radio contours, starting at the specified mJy beam^{-1} level, increase by a factor of 3. The red dashed circle indicates the position of the targeted source (i.e., the optical counterpart). The spectra and finding charts for all the 93 G4Jy-3CRE sources analyzed here are available online.

(The complete figure set (93 images) is available.)

ORCID iDs

A. García-Pérez https://orcid.org/0000-0002-9896-6430
H. A. Peña-Herazo https://orcid.org/0000-0003-0032-9538
A. Jimenez-Gallardo https://orcid.org/0000-0003-4413-7722
V. Chavushyan https://orcid.org/0000-0002-2558-0967
F. Massaro https://orcid.org/0000-0002-1704-9850
S. V. White https://orcid.org/0000-0002-2340-8303
A. Capetti https://orcid.org/0000-0003-3684-4275
B. Balmaverde https://orcid.org/0000-0002-0690-0638
W. R. Forman https://orcid.org/0000-0002-9478-1682
C. C. Cheung https://orcid.org/0000-0002-4377-0174
C. Mazzucchelli https://orcid.org/0000-0002-5941-5214
N. P. H. Nesvadba https://orcid.org/0000-0001-5783-6544
I. Andruchow https://orcid.org/0000-0003-1562-5188
S. Cellone https://orcid.org/0000-0002-3866-2726
R. Grossová https://orcid.org/0000-0003-3471-7459
A. Paggi https://orcid.org/0000-0002-5646-2410
E. Sani https://orcid.org/0000-0002-3140-4070
V. Reynaldi https://orcid.org/0000-0002-6472-6711
R. P. Kraft https://orcid.org/0000-0002-0765-0511

References

Abbott, T. M. C., Abdalla, F. B., Allam, S., et al. 2018, ApJS, 239, 18
Abell, G. O. 1958, ApJS, 3, 211
Abell, G. O., Corwin, H. G. J., & Olowin, R. P. 1989, ApJS, 70, 1
Ahn, C. P., Alexandroff, R., Allende Prieto, C., et al. 2012, ApJS, 203, 21
Aldinucci, M., Bagnasco, S., Lusso, S., et al. 2017, JPhCS, 898, 082039
Allison, J. R., Sadler, E. M., & Meekin, A. M. 2014, MNRAS, 440, 696
Bacon, R., Accardo, M., Adjali, L., et al. 2010, Proc. SPIE, 7735, 773508
Baldi, R. D., Rodríguez Zaurín, J., Chiaberge, M., et al. 2019, ApJ, 870, 53
Baldwin, J. A. 1975, ApJ, 201, 26
Bechtold, J., Dobrzycki, A., Wilden, B., et al. 2002, ApJS, 140, 143
Bennett, A. S. 1962, MmRAS, 68, 163
Bennett, C. L., Larson, D., Weiland, J. L., & Hinshaw, G. 2014, ApJ, 794, 135
Best, P. N., Röttgering, H. J. A., & Lehnert, M. D. 1999, MNRAS, 310, 223
Bolton, J. G., Savage, A., & Wright, A. E. 1979, AuJPA, 46, 1
Burbidge, E. M. 1968, ApJL, 154, L109
Burbidge, E. M., & Burbidge, G. R. 1972, ApJ, 172, 37
Burbidge, E. M., & Kinman, T. D. 1966, ApJ, 145, 654
Burgess, A. M., & Hunstead, R. W. 2006, AJ, 131, 114
Buttiglione, S., Capetti, A., Celotti, A., et al. 2010, A&A, 509, A6
Cava, A., Bettoni, D., Poggianti, B. M., et al. 2009, A&A, 495, 707
Clarke, M. E. 1964, MNRAS, 127, 405
Clemens, J. C., Crain, J. A., & Anderson, R. 2004, Proc. SPIE, 5492, 331

Cohen, A. S., Lane, W. M., Cotton, W. D., et al. 2007, AJ, 134, 1245
Condon, J. J., Cotton, W. D., Greisen, E. W., et al. 1998, AJ, 115, 1693
Costero, R., & Osterbrock, D. E. 1977, ApJ, 211, 675
Croom, S. M., Smith, R. J., Boyle, B. J., et al. 2004, MNRAS, 349, 1397
Croston, J. H., Hardcastle, M. J., Harris, D. E., et al. 2005, ApJ, 626, 733
da Costa, L. N., Pellegrini, P. S., Davis, M., et al. 1991, ApJS, 75, 935
Danziger, I. J., & Goss, W. M. 1983, MNRAS, 202, 703
Douglas, J. N., Bash, F. N., Bozyan, F. A., Torrence, G. W., & Wolfe, C. 1996, AJ, 111, 1945
Drouart, G., De Breuck, C., Vernet, J., et al. 2012, A&A, 548, A45
Duchesne, S. W., Thomson, A. J. M., Pritchard, J., et al. 2023, PASA, 40, e034
Edge, D. O., Shakeshaft, J. R., McAdam, W. B., Baldwin, J. E., & Archer, S. 1959, MmRAS, 68, 37
Eracleous, M., & Halpern, J. P. 2004, ApJS, 150, 181
Flewelling, H. A., Magnier, E. A., Chambers, K. C., et al. 2020, ApJS, 251, 7
Fouque, P., Durand, N., Bottinelli, L., Gouguenheim, L., & Paturel, G. 1990, A&AS, 86, 473
García-Pérez, A., Peña-Herazo, H. A., Massaro, F., et al. 2023, AJ, 165, 127
Garilli, B., Maccagni, D., & Tarenghi, M. 1993, A&AS, 100, 33
Ghaffari, Z., Haas, M., Chiaberge, M., et al. 2021, A&A, 653, A44
Gill, A., Boyce, M. M., O'Dea, C. P., et al. 2021, ApJ, 912, 88
Gilmozzi, R., & Spyromilio, J. 2007, Msngr, 127, 11
Goncalves, A. C., Veron, P., & Veron-Cetty, M. P. 1998, A&AS, 127, 107
Griffith, M. R., & Wright, A. E. 1993, AJ, 105, 1666
Hale, C. L., McConnell, D., Thomson, A. J. M., et al. 2021, PASA, 38, e058
Hardcastle, M. J., & Worrall, D. M. 2000, MNRAS, 314, 359
Henriksen, M., Harms, R., Burbidge, M., et al. 1991, BAAS, 23, 1423
Hine, R. G., & Longair, M. S. 1979, MNRAS, 188, 111
Ho, L. C., & Kim, M. 2009, ApJS, 184, 398
Holt, J., Tadhunter, C. N., & Morganti, R. 2008, MNRAS, 387, 639
Hurley-Walker, N., Callingham, J. R., Hancock, P. J., et al. 2017, MNRAS, 464, 1146
Ineson, J., Croston, J. H., Hardcastle, M. J., et al. 2013, ApJ, 770, 136
Intema, H. T., Jagannathan, P., Mooley, K. P., & Frail, D. A. 2017, A&A, 598, 78
Jarvis, M. J., Rawlings, S., Eales, S., et al. 2001, MNRAS, 326, 1585
Jimenez-Gallardo, A., Massaro, F., Paggi, A., et al. 2021, ApJS, 252, 31
Jimenez-Gallardo, A., Sani, E., Ricci, F., et al. 2022, ApJ, 941, 114
Jones, D. H., Read, M. A., Saunders, W., et al. 2009, MNRAS, 399, 683
Jones, D. H., Saunders, W., Colless, M., et al. 2004, MNRAS, 355, 747
Jones, P. A., & McAdam, W. B. 1992, ApJS, 80, 137
Joye, W. A., & Mandel, E. 2003, in ASP Conf. Ser. 295, Astronomical Data Analysis Software and Systems XII, ed. H. E. Payne, R. I. Jedrzejewski, & R. N. Hook (San Francisco, CA: ASP), 489
Ivezić, Ž., Kahn, S. M., Tyson, J. A., et al. 2019, ApJ, 873, 111
Kaldare, R., Colless, M., Raychaudhury, S., & Peterson, B. A. 2003, MNRAS, 339, 652
Kinman, T. D., & Burbidge, E. M. 1967, ApJL, 148, L59
Kotyla, J. P., Chiaberge, M., Baum, S., et al. 2016, ApJ, 826, 46
Lacy, M., Baum, S. A., Chandler, C. J., et al. 2020, PASP, 132, 035001
Laing, R. A., Jenkins, C. R., Wall, J. V., & Unger, S. W. 1994, in ASP Conf. Ser. 54, The Physics of Active Galaxies, ed. G. V. Bicknell, M. A. Dopita, & P. J. Quinn (San Francisco, CA: ASP), 201
Laing, R. A., Riley, J. M., & Longair, M. S. 1983, MNRAS, 204, 151
Landoni, M., Massaro, F., Paggi, A., et al. 2015, AJ, 149, 163
Large, M. I., Mills, B. Y., Little, A. G., Crawford, D. F., & Sutton, J. M. 1981, MNRAS, 194, 693
Law-Green, J. D. B., Leahy, J. P., Alexander, P., et al. 1995, MNRAS, 274, 939
Lilly, S. J., & Longair, M. S. 1984, MNRAS, 211, 833
Lynds, C. R. 1967, ApJ, 147, 837
Marziani, P., Sulentic, J. W., Dultzin-Hacyan, D., Calvani, M., & Moles, M. 1996, ApJS, 104, 37
Massaro, F., Chiaberge, M., Grandi, P., et al. 2009, ApJL, 692, L123
Massaro, F., Harris, D. E., Liuzzo, E., et al. 2015b, ApJS, 220, 5
Massaro, F., Harris, D. E., Tremblay, G. R., et al. 2010, ApJ, 714, 589
Massaro, F., Landoni, M., D'Abrusco, R., et al. 2015a, A&A, 575, A124
Massaro, F., Missaglia, V., Stuardi, C., et al. 2018, ApJS, 234, 7
Massaro, F., White, S. V., García-Pérez, A., et al. 2023a, ApJS, 265, 32
Massaro, F., White, S. V., Paggi, A., et al. 2023b, ApJS, 268, 32
Mauch, T., Murphy, T., Buttery, H. J., et al. 2003, MNRAS, 342, 1117
McCarthy, P. J., Kapahi, V. K., van Breugel, W., et al. 1996, ApJS, 107, 19
McConnell, D., Hale, C. L., Lenc, E., et al. 2020, PASA, 37, e048
McMullin, J., Diamond, P., McPherson, A., et al. 2020, Proc. SPIE, 11445, 1144512
Melnick, J., & Quintana, H. 1981, A&AS, 44, 87
Menzies, J. W., Coulson, I. M., & Sargent, W. L. W. 1989, AJ, 97, 1576
Mingo, B., Hardcastle, M. J., Croston, J. H., et al. 2014, MNRAS, 440, 269
Missaglia, V., Massaro, F., Liuzzo, E., et al. 2021, ApJS, 255, 18
Morton, D. C., & Tritton, K. P. 1982, MNRAS, 198, 669
Murphy, T., Sadler, E. M., Ekers, R. D., et al. 2010, MNRAS, 402, 2403
Oke, J. B. 1974, ApJS, 27, 21
Oke, J. B., & Gunn, J. E. 1983, ApJ, 266, 713
Owen, F. N., Ledlow, M. J., & Keel, W. C. 1995, AJ, 109, 14
Parisi, P., Masetti, N., Rojas, A. F., et al. 2014, A&A, 561, A67
Peña-Herazo, H. A., Marchesini, E. J., Álvarez Crespo, N., et al. 2017, Ap&SS, 362, 228
Peña-Herazo, H. A., Massaro, F., Chavushyan, V., et al. 2019, Ap&SS, 364, 85
Peña-Herazo, H. A., Paggi, A., García-Pérez, A., et al. 2021, AJ, 162, 177
Peterson, B. A., & Bolton, J. G. 1972, ApJL, 173, L19
Ricci, F., Massaro, F., Landoni, M., et al. 2015, AJ, 149, 160
Rocca-Volmerange, B., Le Borgne, D., De Breuck, C., Fioc, M., & Moy, E. 2004, A&A, 415, 931
Sadler, E. M., Chhetri, R., Morgan, J., et al. 2019, MNRAS, 483, 1354
Safouris, V., Subrahmanyan, R., Bicknell, G. V., & Saripalli, L. 2009, MNRAS, 393, 2
Sandage, A. 1978, AJ, 83, 904
Santoro, F., Tadhunter, C., Baron, D., Morganti, R., & Holt, J. 2020, A&A, 644, A54
Sbarufatti, B., Falomo, R., Treves, A., & Kotilainen, J. 2006, A&A, 457, 35
Scarpa, R., Falomo, R., & Pesce, J. E. 1996, A&AS, 116, 295
Schmidt, M. 1965, ApJ, 141, 1
Schmidt, M. 1966, ApJ, 144, 443
Sejake, P. K., White, S. V., Heywood, I., et al. 2023, MNRAS, 518, 4290
Simpson, C., Clements, D. L., Rawlings, S., & Ward, M. 1993, MNRAS, 262, 889
Spinrad, H., Djorgovski, S., Marr, J., & Aguilar, L. 1985, PASP, 97, 932
Springob, C. M., Haynes, M. P., Giovanelli, R., & Kent, B. R. 2005, ApJS, 160, 149
Stickel, M., Fried, J. W., & Kuehr, H. 1989, A&AS, 80, 103
Tadhunter, C. N., Morganti, R., di Serego Alighieri, S., Fosbury, R. A. E., & Danziger, I. J. 1993, MNRAS, 263, 999
Taylor, M. B. 2005, in ASP Conf. Ser. 347, Astronomical Data Analysis Software and Systems XIV, ed. P. Shopbell, M. Britton, & R. Ebert (San Francisco, CA: ASP), 29
Thompson, D. J., Djorgovski, S., & de Carvalho, R. 1990, PASP, 102, 1235
Tody, D. 1986, Proc. SPIE, 627, 733
Torrealba, J., Chavushyan, V., Cruz-González, I., et al. 2012, RMxAA, 48, 9
Tritton, K. P. 1972, MNRAS, 158, 277
Vagshette, N. D., Naik, S., & Patil, M. K. 2019, MNRAS, 485, 1981
Wayth, R. B., Lenc, E., Bell, M. E., et al. 2015, PASA, 32, e025
Wenger, M., Ochsenbein, F., Egret, D., et al. 2000, A&AS, 143, 9
White, S. V., Franzen, T. M. O., Riseley, C. J., et al. 2020a, PASA, 37, e018
White, S. V., Franzen, T. M. O., Riseley, C. J., et al. 2020b, PASA, 37, e017
Whiteoak, J. B. 1972, AuJPh, 25, 233
Wilkes, B. J. 1986, MNRAS, 218, 331
Wilkes, B. J., Wright, A. E., Jauncey, D. L., & Peterson, B. A. 1983, PASA, 5, 2
Willott, C. J., Rawlings, S., Jarvis, M. J., & Blundell, K. M. 2003, MNRAS, 339, 173
Wills, K. A., Morganti, R., Tadhunter, C. N., Robinson, T. G., & Villar-Martin, M. 2004, MNRAS, 347, 771
Wootten, A., & Thompson, A. R. 2009, IEEEP, 97, 1463
Wright, A. E., Griffith, M. R., Burke, B. F., & Ekers, R. D. 1994, ApJS, 91, 111
Wright, A. E., Jauncey, D. L., Peterson, B. A., & Condon, J. J. 1977, ApJL, 211, L115
Wright, A. E., Peterson, B. A., Jauncey, D. L., & Condon, J. J. 1979, ApJ, 229, 73
Wright, E. L., Eisenhardt, P. R. M., Mainzer, A. K., et al. 2010, AJ, 140, 1868